System B – Cr – O

Determination of Gibbs Energies of Formation of Cr_3B_4, CrB_2, and CrB_4 by Electromotive Force Measurement Using Solid Electrolyte,
H. Yamamoto, Y. Wada, K. Nishiyama, Y. Taniguchi, A. Nozaki, and M. Morishita,
Mater. Trans., Vo.61 (2020), 2357-2362.

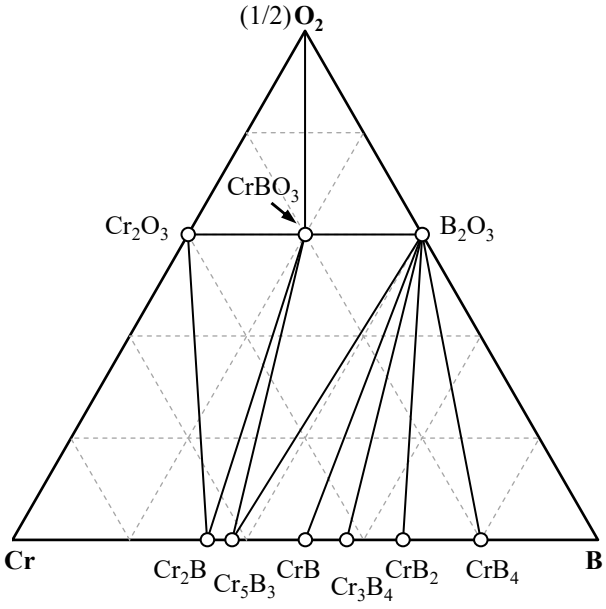

Fig. Phase relationships for the Cr–B–O ternary system at 1273 K.

System B – Cr – O

Determination of Gibbs Energies of Formation of Cr_3B_4, CrB_2, and CrB_4 by Electromotive Force Measurement Using Solid Electrolyte,
H. Yamamoto, Y. Wada, K. Nishiyama, Y. Taniguchi, A. Nozaki, and M. Morishita,
Mater. Trans., Vo.61 (2020), 2357-2362.

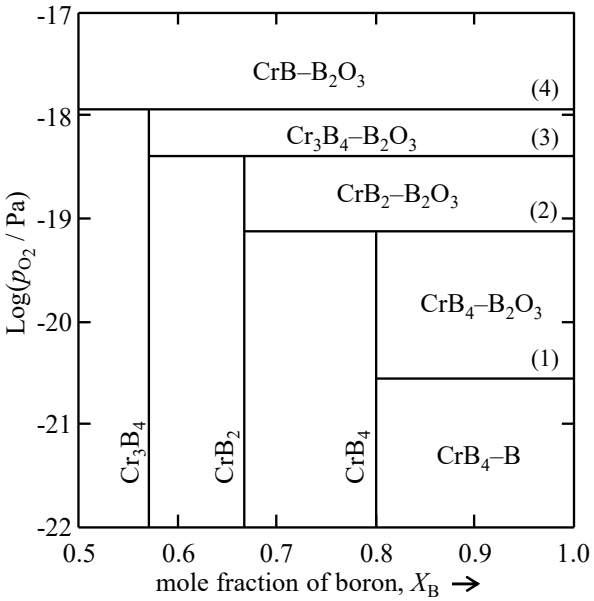

Fig. Composition-oxygen partial pressure diagram of the Cr–B–O ternary system at 1300 K.

System　B - Mo - Ni

Isothermal Phase Diagram of the Ni - Mo－B System,
S.Omori, Y.Hashimoto and K.Koyama,
Kouon Gakkaishi, Vol.7 (1981), pp.162-166.

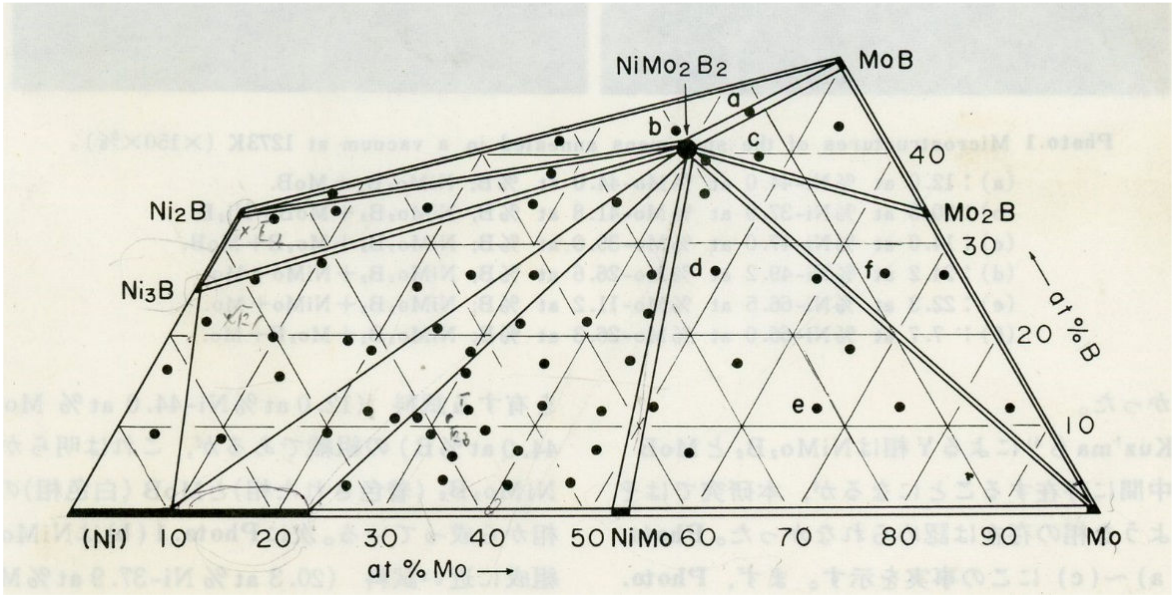

Fig. Isothermal Phase Diagram of the Ni - Mo－B System at 1273 K.

System　B - Mo - Ni

Liquidus Surface of the Ni - Mo－B System,
S.Omori, Y.Hashimoto and K.Koyama,
Kouon Gakkaishi, Vol.7 (1981), pp.167-173.

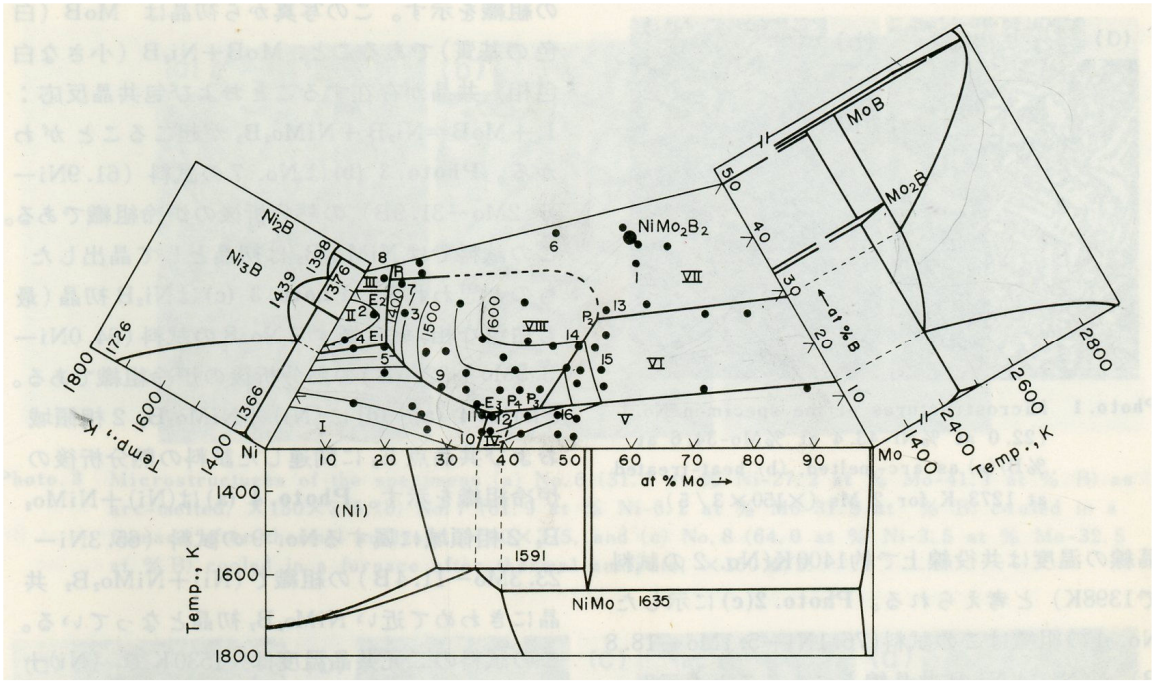

Fig. Liquidus surface of the Ni-Mo-B system in the lower boron region than the Ni_3B-MoB quasi-binary system.

System B - Mo - Ni
Calculated Phase Diagram of the Ni－Mo－B Ternary System, M.Morishita, K.Koyama, S.Yagi and G. Zhang, J. Alloys and Compounds, Vol.314, (2001), pp.214-218.

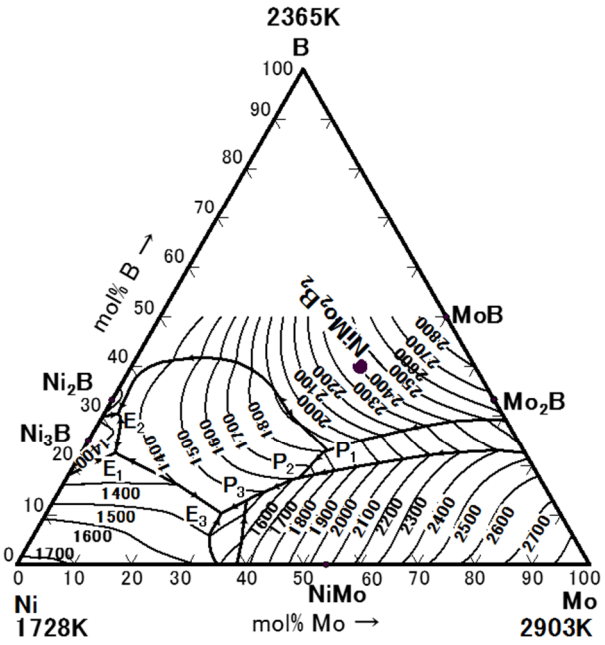

Fig. The calculated Ni-Mo-B ternary phase diagram in the low boron composition range

System B - Mo - Ni - O
Phase Relationship in the Ni - Mo - B - O System and Oxidation Property of a Ni - $NiMo_2B_2$ Two-Phase Alloy, M.Morishita, K.Koyama, K.Maeda and G. Zhang, J. Japan Inst. Met., Vol.65 (2001), pp.279-287.

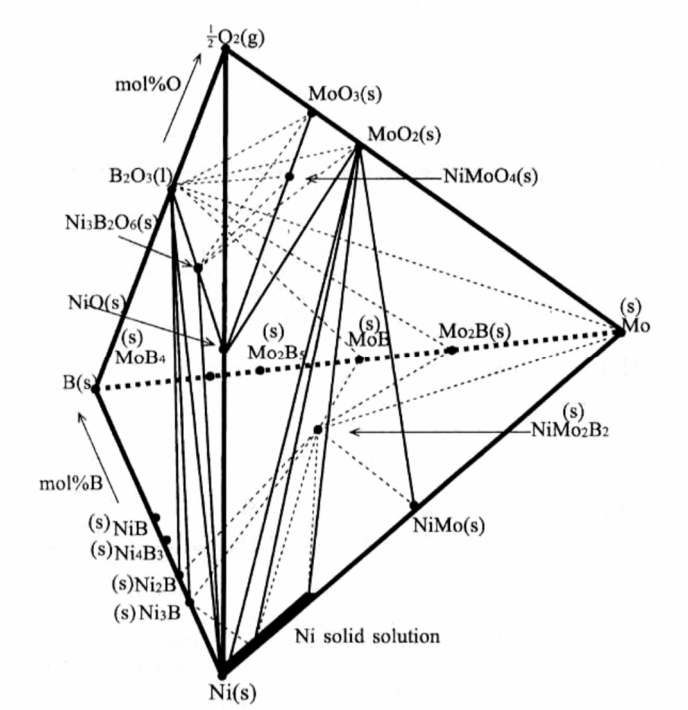

Fig. Phase relationship in the B-Mo-Ni O system at 973 K.

System　B‐Mo‐O

Determination of Gibbs Energy of Formation of Molybdenum-Boron Binary System by Electromotive Force Measurement Using Solid Electrolyte
H. Yamamoto, M. Morishita, T. Yamamoto and K. Furukawa,
Metallurgical and Materials Transactions B, Vol. 42B (2011), pp. 114-120.

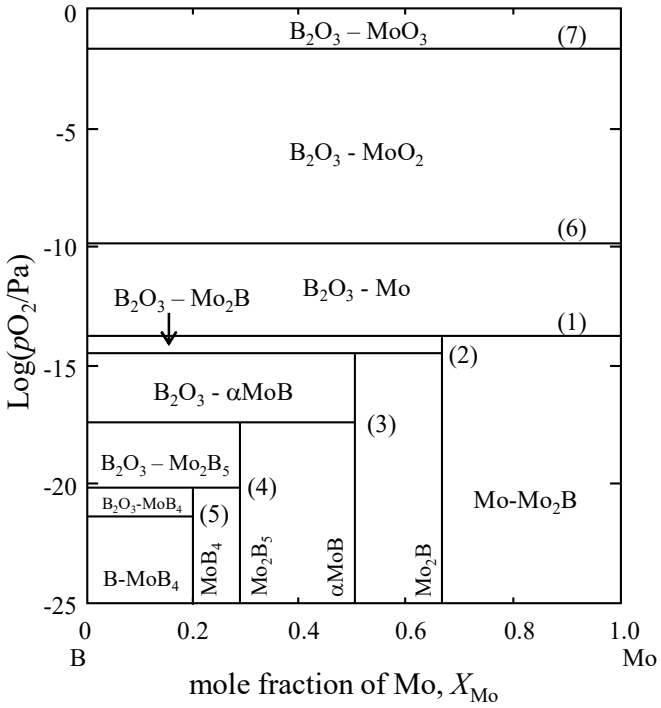

Fig. Composition-oxygen partial pressure diagram of the molybdenum-boron-oxygen system at 1273 K. (1) Mo-Mo_2B-B_2O_3, (2) Mo_2B-MoB-B_2O_3, (3) MoB-Mo_2B_5-B_2O_3, (4) Mo_2B_5-MoB_4-B_2O_3, (5) MoB_4-B-B_2O_3, (6) Mo-MoO_2-B_2O_3, (7) MoO_2-MoO_3-B_2O_3 ternary phase equilibria.

System　B‐Ni

Phase Diagram of Binary Nickel‐Boron System at Nickel Side,
S. Omori, Y.Hashimoto, S.Nakamura, K.Hidaka and Y.Kohira,
J. Japan Soc. Powder Powder Metallurgy, Vo.18 (1971), pp.132-135.

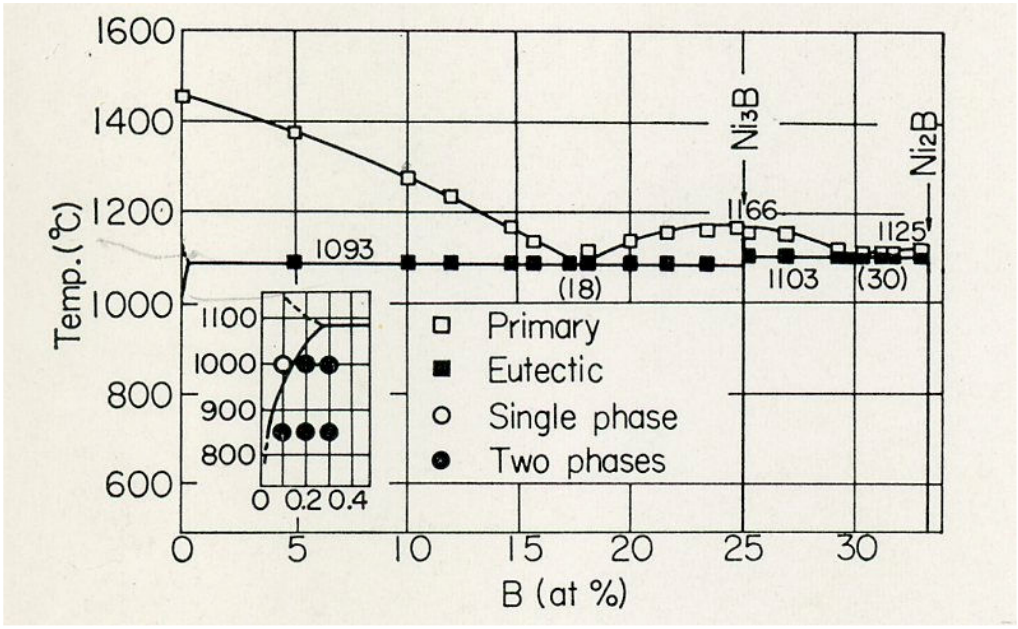

Fig. Phase diagram of Ni‐B system (up to 33.3at%B).

System　B‐Ni‐O

Composition-partial oxygen pressure diagram for Ni-B-O system
H. Yamamoto and M. Morishita,
J. Alloys and Comp., Vol. 438 (2007), pp. L1-L3.

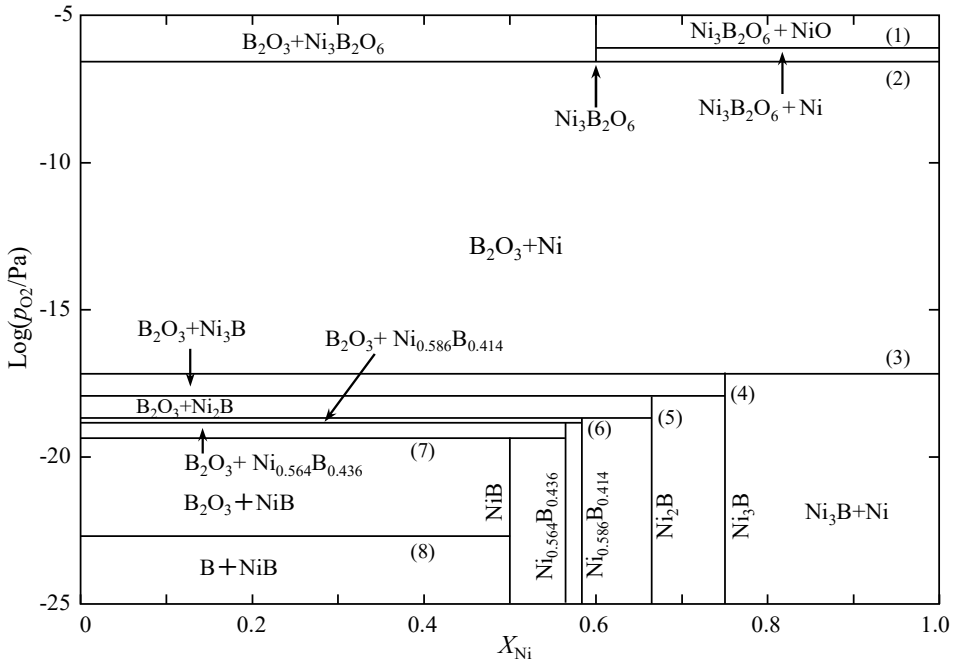

Fig. Composition-oxygen partial pressure diagram for the Ni-B-O system at 1223 K. Horizontal lines represent the equilibrium regions as follows:
(1): Ni-NiO-$Ni_3B_2O_6$, (2): Ni-$Ni_3B_2O_6$-B_2O_3, (3): Ni-Ni_3B-B_2O_3, (4): Ni_3B-Ni_2B-B_2O_3, (5): Ni_2B-$Ni_{0.586}B_{0.414}$-B_2O_3, (6): $Ni_{0.586}B_{0.414}$-$Ni_{0.564}B_{0.436}$-B_2O_3, (7): $Ni_{0.564}B_{0.436}$-NiB-B_2O_3, and (8): B-B_2O_3-NiB.

System B - W - Ni

Calculated Phase Diagram of the Ni－W－B Ternary System,
M.Morishita, K.Koyama, K.Maeda and G. Zhang,
Materials Transactions of the Japan Institute of Metals, Vol.40, (1999), pp.600-605.

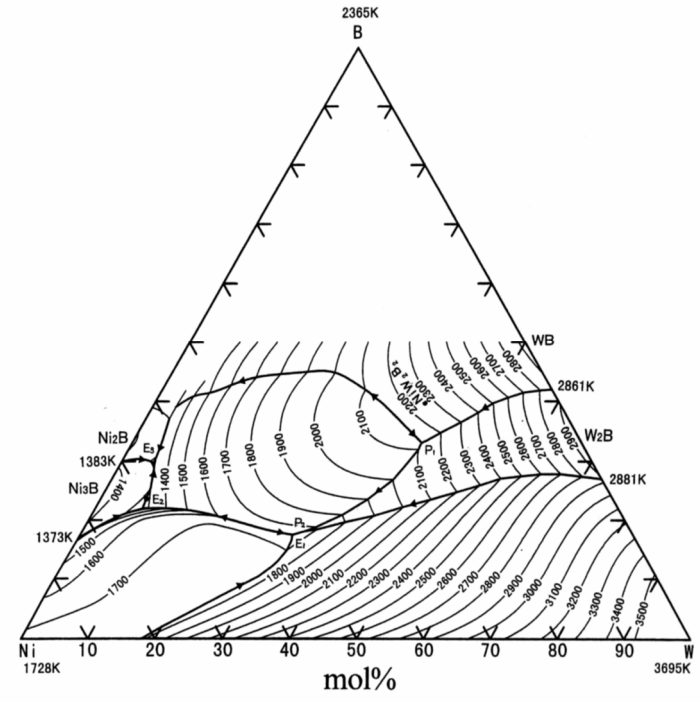

Fig. The calculated Ni-W-B ternary phase diagram in the low boron composition range

System　B‐W‐O

Determination of Gibbs Energy of Mixing of Tungsten-Boron Binary System by Electromotive Force Measurement Using Solid Electrolyte,
H. Yamamoto, M. Morishita, Y. Miyake, and S. Hiramatsu,
Metallurgical and Materials Transactions B, Vol. 48(2017), pp.1703-1714.

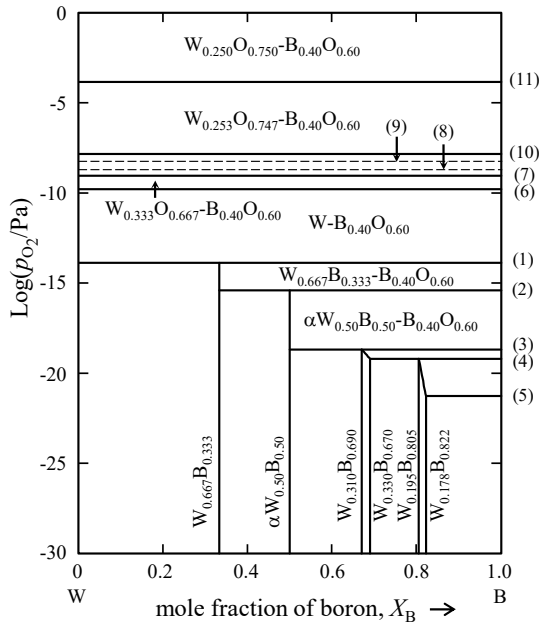

Fig. Composition-oxygen partial pressure diagram of the W-B-O ternary system at 1273 K (1000 °C).

System　C‐Ni‐O‐Ti

Phase Relationships and the Partial Phase Diagram of the Ni‐Ti—C—O System,
Y.Hashimoto, S.Omori, K.Koyama and Y. Arami,
Kouon Gakkaishi, Vol.7 (1981), pp.255-263.

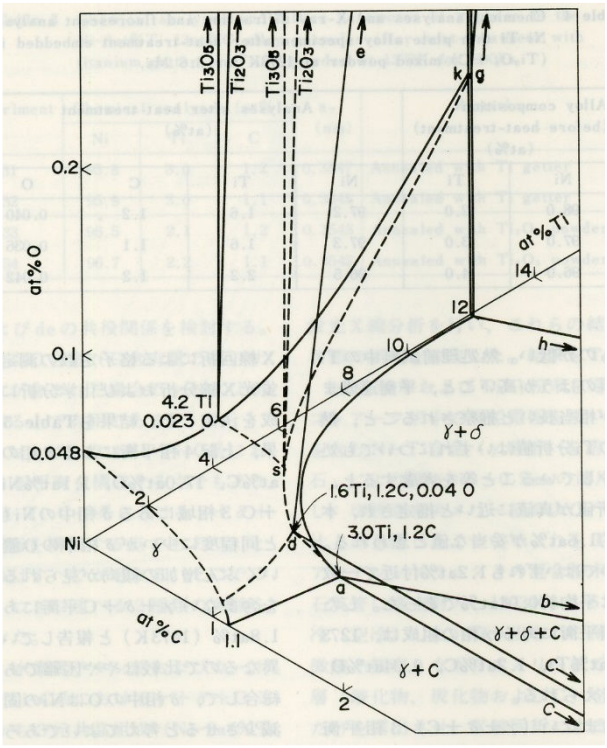

Fig. Isothermal phase diagram in the Ni-rich region of the Ni-Ti-C-O system at 1273 K (Partially drawn).

System　　C－O－Ti
Partial Phase Diagram of the Ti－C－O System in the High Carbon and High Oxygen Region, Y.Hashimoto, S.Omori, K.Koyama and Y. Arami, Kouon Gakkaishi, Vol.7 (1981), pp.209-215.
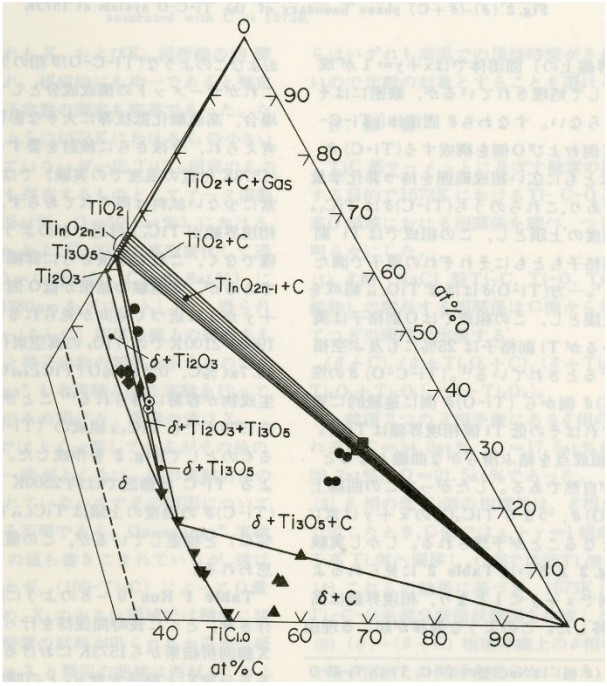   Fig. Isothermal diagram of the Ti-C-O system at 1573 K.

System　　Fe－Mo－O
Determination of Standard Gibbs Energies of Formation of $Fe_2Mo_3O_{12}$, $Fe_2Mo_3O_8$, Fe_2MoO_4, and $FeMoO_4$ of the Fe－Mo－O Ternary System an μ Phase of the Fe－Mo Binary System by Electromotive Force Measurte Using a Y_2O_3-Stabilized ZrO_2 Solid Electrlyte K.Koyama, M.Morishita, T.Harada and N.Maekawa, Metallurgical and Materials Transactions, Vol.B34, (2003), pp.653-659.
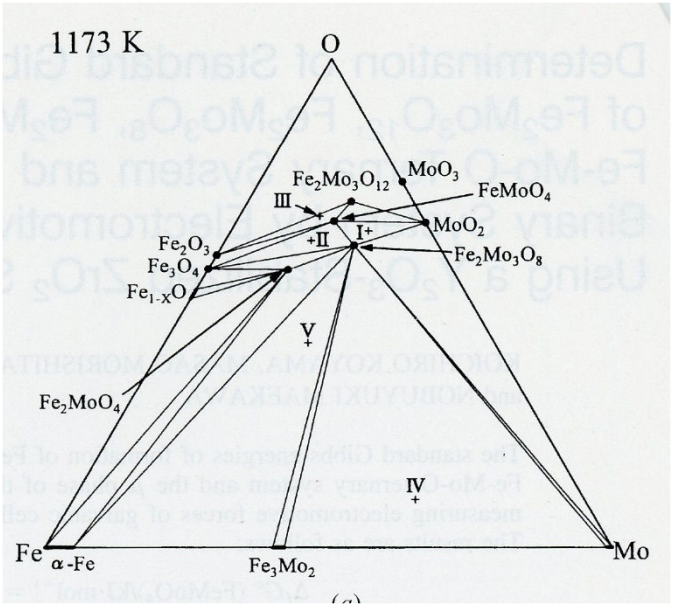   Fig. The compositions of the electrode used for the electromotive force measurements.

System　　Fe - Mo - O
Determination of Standard Gibbs Energies of Formation of $Fe_2Mo_3O_{12}$, $Fe_2Mo_3O_8$, Fe_2MoO_4, and $FeMoO_4$ of the Fe－Mo－O Ternary System an μ Phase of the Fe－Mo Binary System by Electromotive Force Measurte Using a Y_2O_3-Stabilized ZrO_2 Solid Electrlyte K.Koyama, M.Morishita, T.Harada and N.Maekawa, Metallurgical and Materials Transactions, Vol.B34, (2003), pp.653-659.
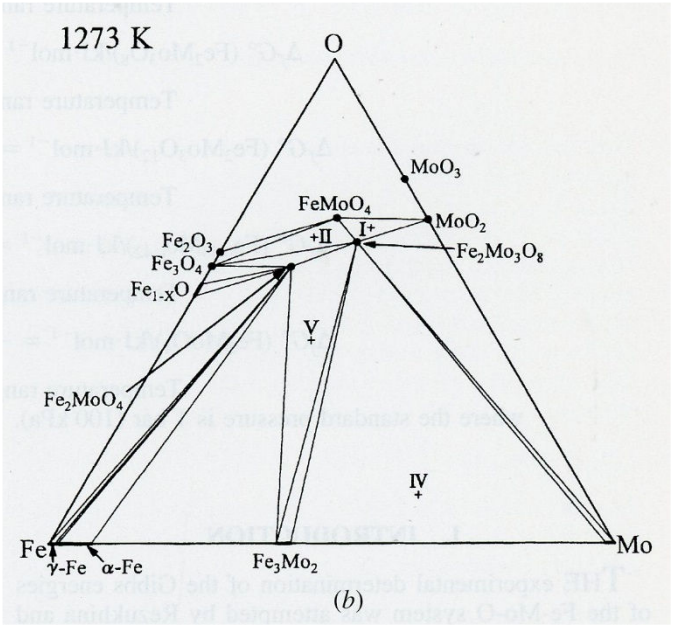 Fig. The compositions of the electrode used for the electromotive force measurements.

System　　KCl - LiCl - $MgCl_2$
Phase Diagram of LiCl-KCl-$MgCl_2$ Ternary System in Low $MgCl_2$ composition, M.Morishita, M. Murase and K.Koyama, J. Japan Inst. Met., Vol.59 (1995), pp.799-805.
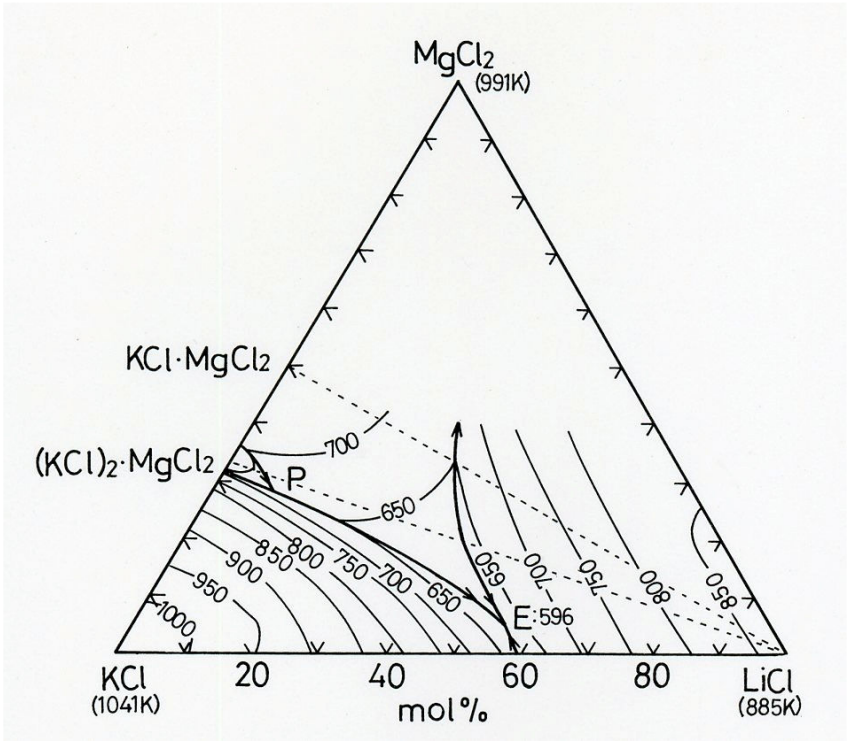 Fig. Phase diagram of the LiCl-KCl-$MgCl_2$ ternary system in low $MgCl_2$ composition.

System Mo - Ni - O

Calorimetric Study of Nickel Molybdate: Heat Capacity, Enthalpy and Gibbs Energy of Formation,
M.Morishita and A.Navrotsky,
Journal of the American Ceramic Society, Vol.86, (2003), Vol.1927-1932.

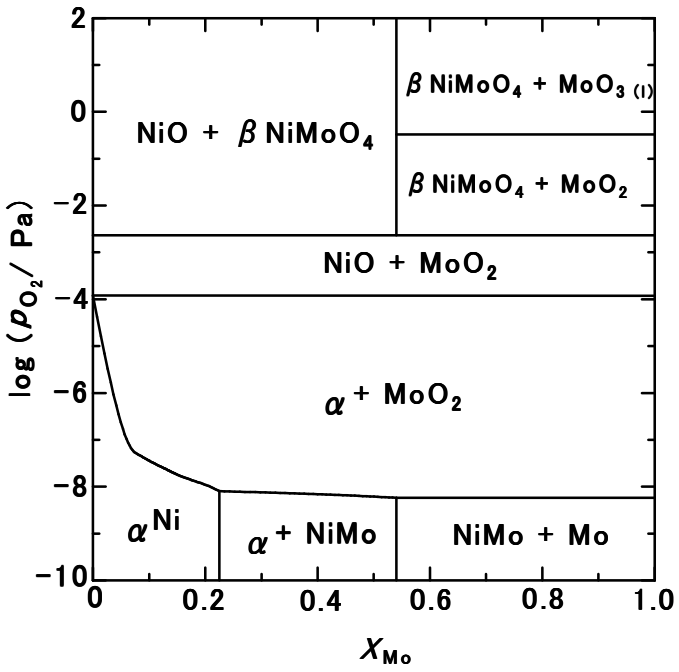

Fig. Composition-partial pressure diagram for the Ni-Mo-O ternary system at 1373 K.